ACS OMEGA

http://pubs.acs.org/journal/acsodf

Article

Implementation of Oxy-Fuel Combustion (OFC) Technology in a Gasoline Direct Injection (GDI) Engine Fueled with Gasoline–Ethanol Blends

Xiang Li,* Yiqiang Pei, Dayou Li, Tahmina Ajmal, Abdel Aitouche, Raouf Mobasheri, and Zhijun Peng*

Cite This: *ACS Omega* 2021, 6, 29394–29402

Read Online

ACCESS | Metrics & More | Article Recommendations

ABSTRACT: Nowadays, to mitigate the global warming problem, the requirement of carbon neutrality has become more urgent. Oxy-fuel combustion (OFC) has been proposed as a promising way of carbon capture and storage (CCS) to eliminate carbon dioxide (CO_2) emissions. This article explores the implementation of OFC technology in a practical gasoline direct injection (GDI) engine fueled with gasoline–ethanol blends, including E0 (gasoline), E25 (25% ethanol, 75% is gasoline in mass fraction), and E50 (50% ethanol, 50% is gasoline in mass fraction). The results show that with a fixed spark timing, φ_{CA50} (where 50% fuel is burned), of E50 and E25 is about 4.5 and 1.9° later than that of E0, respectively. Ignition delay (θ_F) and combustion duration (θ_C) can be extended with the increase of the ethanol fraction in the blended fuel. With the increase of the oxygen mass fraction (OMF) from 23.3 to 29%, equivalent brake-specific fuel consumption ($BSFC_E$) has a benefit of 2.12, 1.65, and 1.51% for E0, E25, and E50, respectively. The corresponding increase in brake-specific oxygen consumption (BSOC) is 21.83, 22.42, and 22.58%, respectively. Meanwhile, θ_F, θ_C, and the heat release rate (HRR) are not strongly affected by the OMF. With the increase of the OMF, the increment of θ_F is 0.7, 1.8, and 2.2° for E0, E25, and E50, respectively. θ_C is only extended by 1, 1.1, and 1.4°, respectively. Besides, by increasing the intake temperature (T_I) from 298 to 358 K under all of the fuel conditions, $BSFC_E$ and BSOC present slight growth trends; θ_F and θ_C are slightly reduced; in the meantime, φ_{CA50}, φ_{Pmax} (crank angle of peak cylinder pressure), and the position of the HRR peak are advanced by nearly 1°.

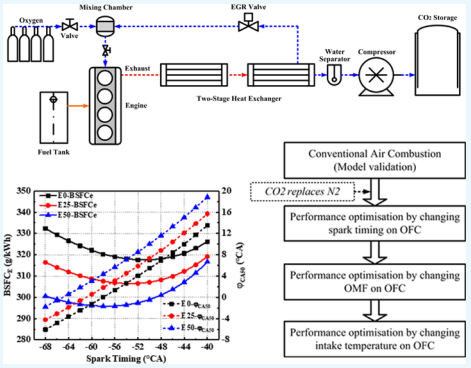

1. INTRODUCTION

Climate change, particularly global warming, has been a serious problem, which causes a wide range of effects on the environment. Hence, carbon neutrality has been proposed as an urgent need to limit global warming by reducing greenhouse gas (GHG) emissions.[1−4] Aiming at reducing the emissions of primary long-lived GHG carbon dioxide (CO_2), oxy-fuel combustion (OFC) technology is helpful in achieving carbon capture and storage (CCS) in conventional internal combustion engines (ICEs) fueled with fossil fuels.[5−8] OFC technology was proposed by Yaverbaum,[5] and the chemical reaction process is shown in eq 1. It presents that the major advantage of OFC is the avoidance of emissions related to the nitrogen element so that the engine exhaust emissions mostly comprise CO_2 and H_2O. Then, H_2O is condensed and separated with a condenser and a gas/water separator. A portion of the remaining CO_2 is recirculated back to the cylinders for utilization. Meanwhile, the rest of the CO_2 is compressed, captured, and stored. The physicochemical properties of CO_2 and nitrogen are listed in Table 1, which render OFC quite different from conventional air combustion (CAC).[9,10]

$$C_xH_y + \left(x + \frac{y}{4}\right)O_2 \rightarrow xCO_2 + \frac{y}{2}H_2O \quad (1)$$

In 1999, Bilger[6] introduced a novel system named the internal combustion Rankine cycle (ICRC), initiating the application of OFC technology into spark ignition (SI) ICEs. In the ICRC system, CO_2 with oxygen enters into the engine combustion chambers. The other prominent characteristic is that water is directly injected into the chambers near the top dead center to control combustion. Over the last decade, Wu et al.[11−14] provided valuable inputs into OFC research, which indicated that the power, fuel economy, and emissions could be improved through optimization strategies in the ICRC port fuel injection (PFI) engine fueled with propane. Li et al.[15,16] explored the potential of the intake charge to optimize

Received: June 5, 2021
Accepted: October 14, 2021
Published: October 27, 2021

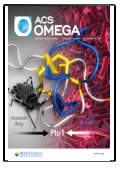

Table 1. Gas Physicochemical Properties at 1000 K and 0.1 MPa[9,10]

property	CO_2	nitrogen	ratio (CO_2/nitrogen)
molecular weight	44	28	1.57
density (kg/m^3)	0.5362	0.3413	1.57
kinematic viscosity (m^2/s)	7.69×10^{-5}	1.2×10^{-4}	0.631
specific heat capacity (kJ/kg K)	1.2343	1.1674	1.06
thermal conductivity (W/m K)	7.057×10^{-2}	6.599×10^{-2}	1.07
thermal diffusivity (m^2/s)	1.1×10^{-4}	1.7×10^{-4}	0.644
mass diffusivity of O_2 (m^2/s)	9.8×10^{-5}	1.3×10^{-4}	0.778
Prandtl number	0.7455	0.7022	1.06
emissivity and absorptivity	>0	~0	

combustion and performance of the OFC SI engine fueled with gasoline.

In summary, most studies on OFC technology in SI engines mainly focused on PFI engines fueled with propane. However, a few studies have been conducted on gasoline direct injection (GDI) engines. The GDI technique is widely known to be the mainstream of SI engines.[17−22] Furthermore, to meet the more stringent standards by reducing vehicular emissions, alcohols have been promising alternative fuels and are widely used as fuel blending components nowadays.[23−29] However, the impacts of OFC implementation in a GDI engine fueled with gasoline−ethanol blends are still unknown.

Hence, the study aimed to explore and provide a deeper understanding of the implementation of OFC technology in a practical GDI engine fueled with gasoline−ethanol blends. This study is a small part of an ongoing "RIVER" project funded by the European Regional Development Fund (ERDF), which aims to develop a novel noncarbon riverboat powered by an ICE with conventional hydrocarbon liquid fuels. In this project, a designed system of OFC with CCS in the application of ICEs is depicted in Figure 1. To achieve noncarbon emissions, pure oxygen is mixed with recirculated exhaust gas (CO_2) prior to entering the engine combustion chambers. Meanwhile, the excess CO_2 would be captured and eventually stored in a storage tank.

2. SIMULATION METHODOLOGY

2.1. Engine Testbed. The numerical study is performed with a turbocharged 2.0 L GDI engine, and the specifications and testbed are illustrated in Table 2 and Figure 2, respectively.

Table 2. Engine Specifications

items	content
engine type	4-cylinder, 4-stroke
bore × stroke (mm)	82.5 × 92
displacement (L)	2.0
injection type	GDI
intake type	turbocharged
compression ratio	9.6:1
rated speed (rpm)	5500
rated power (kW)	160
maximum Torque (N·m)	320

The required data for model validation were obtained from the engine testbed under CAC mode. The engine speed and torque can be accurately controlled and measured by a programmable electronic control unit (ECU) and an electrical dynamometer. In addition, spark-plug-type pressure sensors (AVL-GH13Z), a charge amplifier (Kistler 5018A), and a combustion analyzer (AVL 641) were utilized to measure, analyze, and record the transient cylinder pressure signals. The cylinder pressure should be averaged by 200 consecutive cycles to reduce the deviation of cycle-to-cycle variations. According to Holman's root mean square method, the uncertainties of

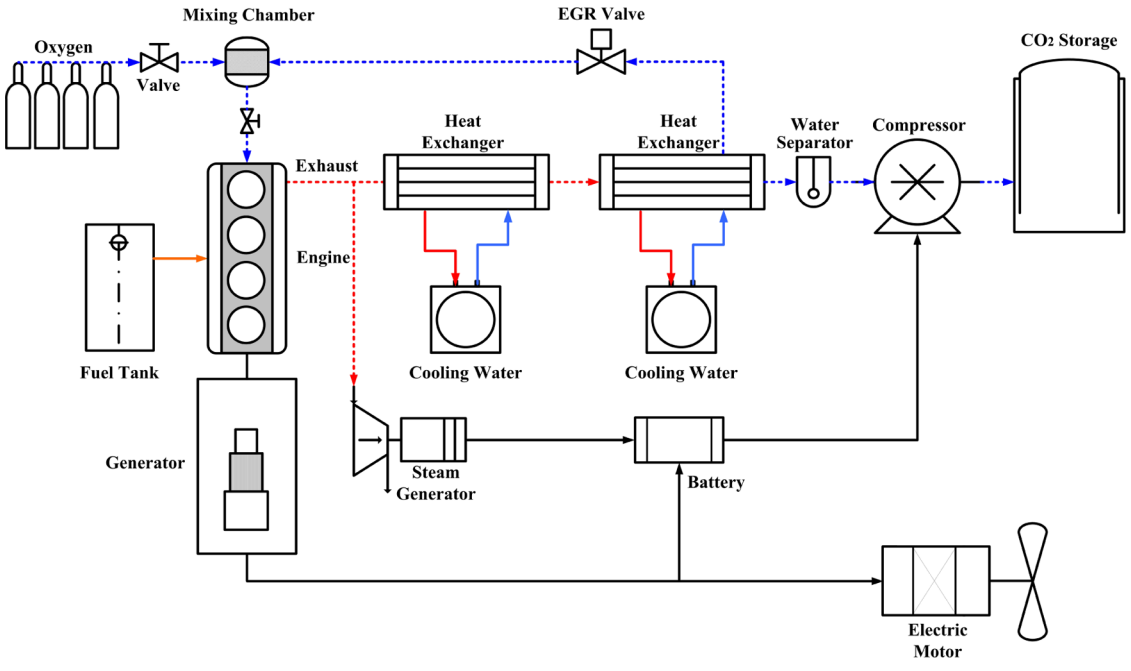

Figure 1. Schematic of OFC in the application of an ICE with CCS.

https://doi.org/10.1021/acsomega.1c02947
ACS Omega 2021, 6, 29394−29402

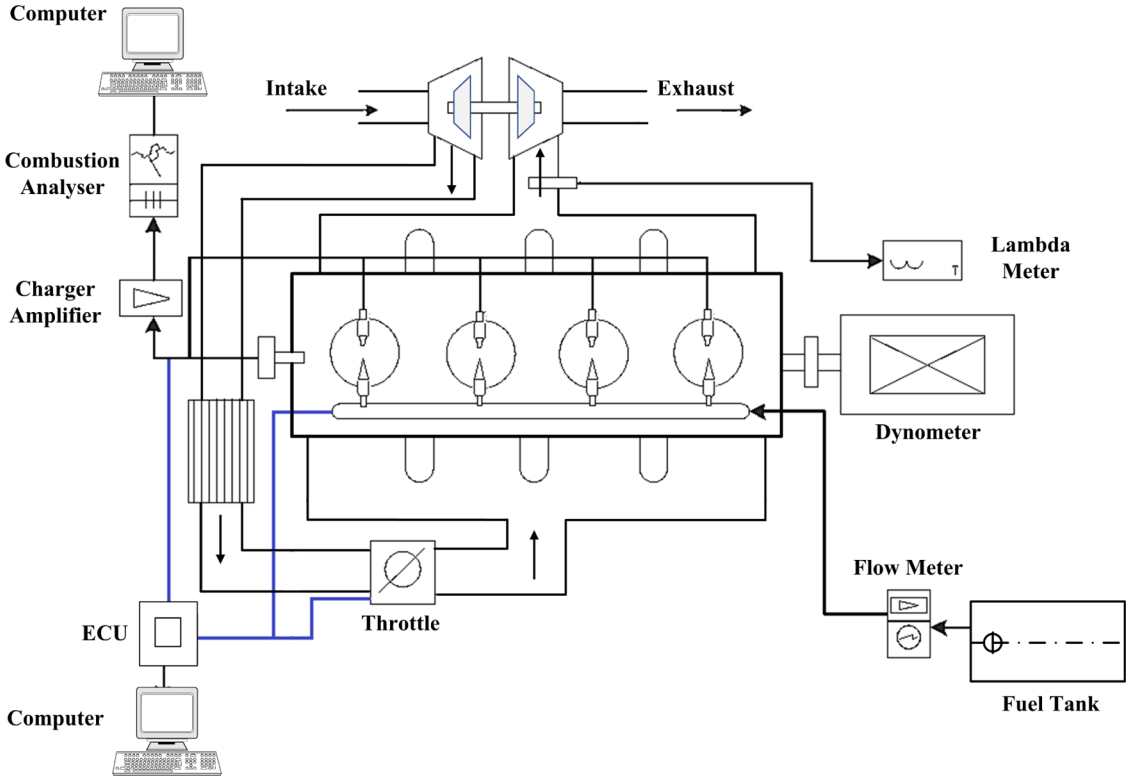

Figure 2. Schematic of the engine testbed.

some items are listed in Table 3.[30] Besides, the spark timings were optimized to be the minimum advance for maximum brake torque (MBT) or the knock-limited spark advance (KLSA). The fuels used in this study include E0 (gasoline), E25 (25% ethanol, 75% is gasoline in mass fraction), and E50 (50% ethanol, 50% is gasoline in mass fraction), which are mixed to ensure they are completely miscible before the test. The fuel properties of gasoline and ethanol used are presented in Table 4.

Table 3. Uncertainties of Measured Parameters

measured parameters	uncertainty (%)
engine speed	±0.1
BMEP	±0.1
BSFC	±0.2
cylinder pressure	±0.1
λ	±0.3
coolant temperature	±0.4
intercooler output temperature	±0.4

Table 4. Fuel Properties

fuel type	ethanol	gasoline
chemical formula	C_2H_5OH	C5−C12
relative molecular mass	46	95−120
gravimetric oxygen content (%)	34.78	<1
research octane number	107	95
density (20 °C) (kg/L)	0.789	0.73
dynamic viscosity (20 °C) (mPa·s)	1.2	0.52
kinematic viscosity (20 °C) (mm^2/s)	1.52	0.71
surface tension (20 °C) (N/m)	21.97	22
boiling range (°C)	78	30−200
low heating value (kJ/kg)	26 900	44 300
latent heat of vaporization (kJ/kg)	840	370
laminar flame speed (20 °C) (m/s)	0.5	0.33
stoichiometric air−fuel ratio	8.95	14.7

2.2. Model Description and Research Approach. The one-dimensional model of this numerical study is established by GT-Power, which is commonly used in academia in the research of SI engines.[31−33] The main submodels are the "Woschni model"[34] and the "SI turbulent flame combustion model."[35] The heat transfer coefficient h and laminar flame speed S_L are presented in eqs 2 and 3, respectively.

$$h = 110d^{-0.2}P^{0.8}T^{-0.53}\left[C_1c_m + C_2\frac{V_ST_1}{P_1V_1}(P - P_0)\right]^{0.8} \quad (2)$$

Here, h denotes the heat transfer coefficient, d denotes the diameter of the cylinder bore, P denotes the cylinder pressure, T denotes the in-cylinder mean gas temperature, C_1 denotes a constant related to the airflow velocity coefficient, C_2 denotes a constant related to the combustion chamber, c_m denotes the mean piston speed, V_S denotes the cylinder volume, and P_0 denotes the cylinder pressure when the engine is started. T_1, P_1, and V_1 are cylinder temperature, pressure, and volume at the beginning of compression, respectively.

$$S_L = [B_m - B_\delta(\delta - \delta_m)^2]\left(\frac{T_u}{T_{ref}}\right)^\alpha\left(\frac{p}{p_{ref}}\right)^\beta f(D) \quad (3)$$

Here, S_L denotes the laminar flame speed, B_m denotes the maximum laminar speed, B_δ denotes the laminar speed roll-off value, δ denotes the in-cylinder equivalence ratio, δ_m denotes the equivalence ratio at the maximum speed, T_u denotes the unburned gas temperature, T_{ref} denotes 298 K, p denotes the pressure, p_{ref} denotes 101.325 kPa, α denotes the temperature

https://doi.org/10.1021/acsomega.1c02947
ACS Omega 2021, 6, 29394−29402

exponent, β denotes the pressure exponent, and $f(D)$ denotes the dilution effect.

In this research, fueled with E0, E25, and E50, the engine runs at 1500 revolutions per minute (rpm) with 10 bar brake mean effective pressure (BMEP), representing a mid-high load of engine operating conditions. The research approach of this study is illustrated in Figure 3.

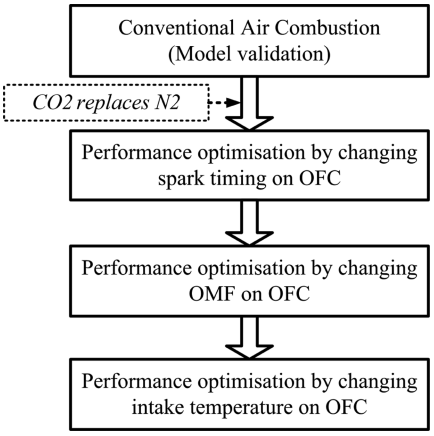

Figure 3. Flow chart of the research approach.

First, model validation is completed based on the experimental data. Second, the optimization of OFC performance by changing spark timing is conducted. In the meantime, the throttle opening angle and stoichiometric air−fuel ratio are held constant. Third, the performance optimization by changing the oxygen mass fraction (OMF) is analyzed. When the OMF changes, the throttle opening angle remains unchanged and the spark timings should be optimized to be the MBT under each OMF condition. Lastly, simulation work is conducted in an attempt to optimize the engine performance by changing the intake temperature.

In this study, ignition delay (θ_F) denotes the crank angle (CA) interval between spark timing and φ_{CA10} (where 10% of the fuel is burned). Combustion duration (θ_C) denotes the CA interval between φ_{CA10} and φ_{CA90} (where 90% of the fuel is burned). Besides, φ_{CA50}, T_M, and φ_{Pmax} are introduced to denote the CA where 50% of the fuel is burned, the maximum in-cylinder temperature, and the CA of the peak cylinder pressure. Brake-specific oxygen consumption (BSOC), equivalent brake-specific fuel consumption ($BSFC_E$), and λ_{O_2} are introduced in eqs 4−6, respectively.

$$BSOC = \frac{\tau_O \times 1000}{P} \tag{4}$$

$$BSFC_E = \frac{\tau_F \times 1000}{P} \times \frac{(\omega_E \times H_E) \times (\omega_G \times H_G)}{H_G} \tag{5}$$

$$\lambda_{O_2} = \frac{\tau_O}{\tau_{ost}} \tag{6}$$

Here, P (kW) denotes the engine brake power. τ_O (kg/h) and τ_F (kg/h) are the consumption rates of oxygen and fuel under actual conditions, respectively. τ_{ost} (kg/h) denotes the oxygen mass flow rate at the stoichiometric condition. ω_E and ω_G are the mass fractions of ethanol and gasoline in the fuel, respectively. H_E and H_G are the low heating values of ethanol and gasoline, respectively.

3. RESULTS AND DISCUSSION

3.1. Model Validation. Figure 4 presents the model validation by a comparison of cylinder pressure between

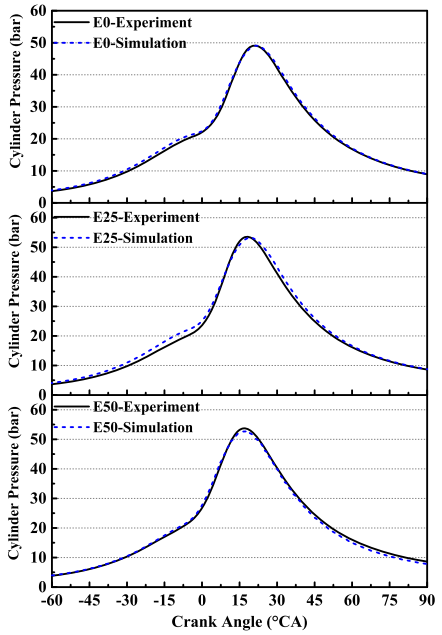

Figure 4. Comparison of cylinder pressure between experimental and simulation results.

experimental and simulation results under E0, E25, and E50 conditions. It can be seen that the curves are in good agreement under all of the conditions. The locations and magnitudes of the curve peak have been well predicted. This indicates that this model is capable of being used for this numerical research.

3.2. Performance Optimization by Changing Spark Timing. This section shows the effects of spark timing on engine combustion performance. Meanwhile, the OMF and T_I are kept at 23.3% and 298 K, respectively.

Figure 5 presents the effects of spark timing on $BSFC_E$ and φ_{CA50}. It can be observed that with the advance of spark timing

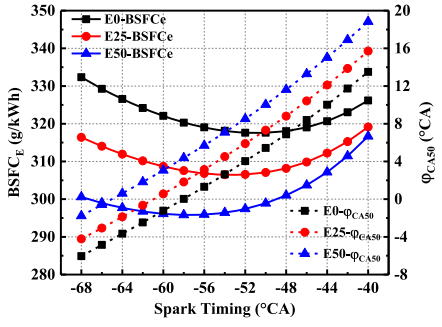

Figure 5. Effects of spark timing on $BSFC_E$ and φ_{CA50}.

from −40 to −68 °CA, the overall trend of $BSFC_E$ initially has a small reduction and then increases. For E0, E25, and E50, the lowest $BSFC_E$ is 317.62, 306.48, and 295.82 g/kWh, which is achieved with the spark timing of −52, −54, and −58 °CA, respectively.

These differences can be observed with the combustion phasing characterized by φ_{CA50}, θ_F, and θ_C. The corresponding

https://doi.org/10.1021/acsomega.1c02947
ACS Omega 2021, 6, 29394−29402

φ_{CA50} values with MBT timing are 4, 4.5, and 4.4 °CA, respectively. Besides, there is a clear contrast between the overall trend of θ_F and θ_C, as shown in Figure 6. By advancing

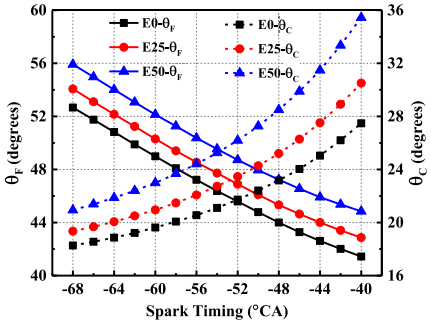

Figure 6. Effects of spark timing on θ_F and θ_C.

spark timing from −40 to −68 °CA, θ_F increases by about 11.2, 11.2, and 11.1° for E0, E25, and E50, respectively. In the meantime, θ_C has a corresponding decline of 9.2, 11.2, and 14.5°. It can be explained by the heat release rate (HRR), an example case with E25 of Figure 7; it also demonstrates that the combustion phasing is very sensitive to spark timing, which leads to a considerable variation in both the location and magnitude of the HRR.

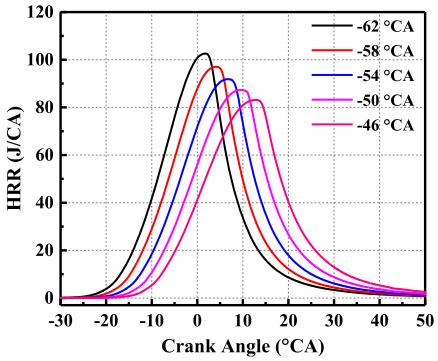

Figure 7. Effects of spark timing on the HRR (E25).

Another important result presented in this section is that with a fixed spark timing, the φ_{CA50} of E50 and E25 is about 4.5 and 1.9° later than that of E0, as shown in Figure 5. Meanwhile, θ_F and θ_C can be extended with the increase of ethanol fraction in the blended fuel. The changes can be attributed to two main reasons by fuel properties, as shown in Table 4. First, the latent heat of vaporization of ethanol is significantly higher than that of gasoline, leading to a stronger cooling effect and suppression of combustion rate. The T_M of E50 is the lowest among the three fuels, while that of E0 is the highest, as shown in Figure 8. Second, the laminar flame speed of ethanol is higher than that of gasoline, which would promote combustion rate and complete combustion. However, the benefit cannot counteract the negative effects of the high latent heat of vaporization of ethanol in this operating condition.

3.3. Performance Optimization by Changing the OMF. This section presents the optimization results on engine combustion performance by changing the OMF. Furthermore, T_I is kept at 298 K, and MBT timing is applied for all operating conditions.

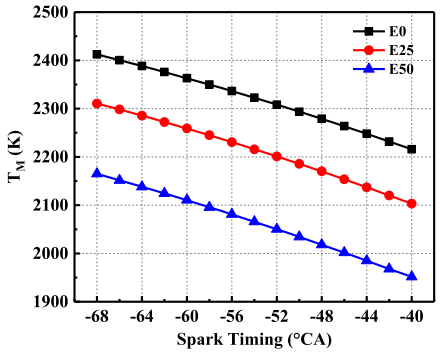

Figure 8. Effects of spark timing on T_M.

Figure 9 shows the effects of the OMF on $BSFC_E$ and BSOC. The OMF is limited to 29% in this study because the

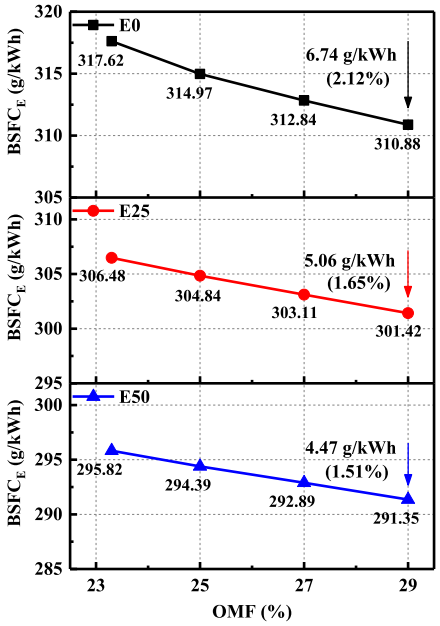

Figure 9. Effects of the OMF on $BSFC_E$.

cost of oxygen supplements should be considered in practical applications. It is set to be 23.3, 25, 27, and 29%, and the corresponding λ_{O_2} is 1, 1.073, 1.159, and 1.245, respectively. Furthermore, the spark timings are optimized to be MBT under each OMF condition.

It can be observed that both the $BSFC_E$ and BSOC are sensitive to the change of the OMF. With the increase of the OMF to 29%, the reduction of $BSFC_E$ is 6.74, 5.06, and 4.47 g/kWh for E0, E25, and E50, which is a saving rate of 2.12, 1.65, and 1.51%, respectively. This benefit is mainly because the specific heat ratio is heightened with the increased OMF, resulting in higher conversion efficiency and stronger work per unit mass of fuel.[35] Besides, the general trend of BSOC is opposite to that of $BSFC_E$. Under the condition of E0, E25, and E50, there is an increase of 21.83, 22.42, and 22.58% in BSOC, respectively. It means that the growing consumption of oxygen should also be considered under higher OMF conditions. Hence, the cost from higher BSOC should be considered with the increase of the OMF.

Figure 10 presents the effects of the OMF on θ_F and θ_C. It can be seen that both θ_F and θ_C are not strongly affected by the

https://doi.org/10.1021/acsomega.1c02947
ACS Omega 2021, 6, 29394−29402

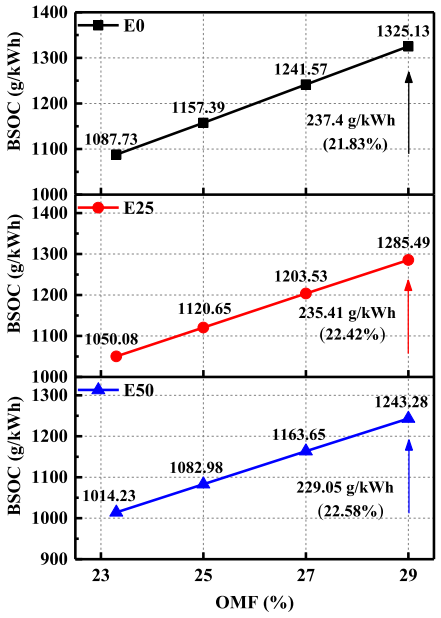

Figure 10. Effects of the OMF on BSOC.

OMF. With the increase of the OMF, the increment of θ_F is 0.7, 1.8, and 2.2° for E0, E25, and E50, respectively. Meanwhile, θ_C is only extended by 1, 1.1, and 1.4°, respectively (Figure 11). This is mainly attributed to the negative impact of

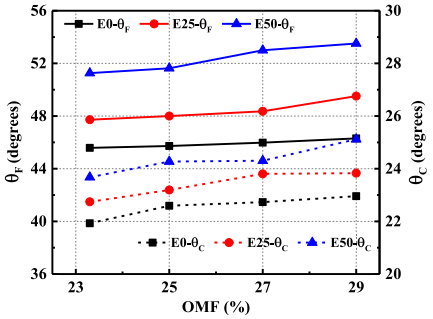

Figure 11. Effects of the OMF on θ_F and θ_C.

the lean fuel−air mixture (λ_{O_2}> 1.1) on laminar burning velocity on increasing the OMF to 27 or 29%, although the impact is partially offset by the influence of decreasing CO_2 fraction in the intake.[35,36] This can also be further explained by the HRR, an example case with E25 in Figure 12. It demonstrates that there is no apparent discrepancy in the HRR on increasing the OMF. The peak of the HRR is just slightly decreased by 2.5 J/CA and delayed by 1.5°.

3.4. Performance Optimization by Changing the Intake Temperature. In this section, the simulation work is conducted in an attempt to optimize the engine performance by changing the intake temperature from 298 to 358 K. Furthermore, the OMF conditions are selected with 23.3 and 29%, and the spark timings are optimized to be MBT.

Figure 13 and Figure 14 show the effects of T_I on $BSFC_E$ and BSOC, respectively. It can be seen that with the increase of T_I from 298 to 358 K, all of the curves of $BSFC_E$ and BSOC present steady but slight growth trends. Hence, an analysis of normalization is also depicted in Figure 13 to show the comparisons with the condition of T_I = 298 K. The average increase rate is, respectively, 0.28 and 0.23% for OMF = 23%

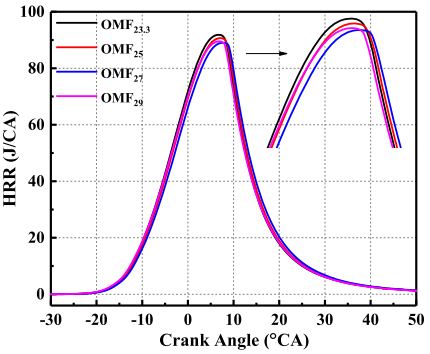

Figure 12. Effects of the OMF on the HRR (E25).

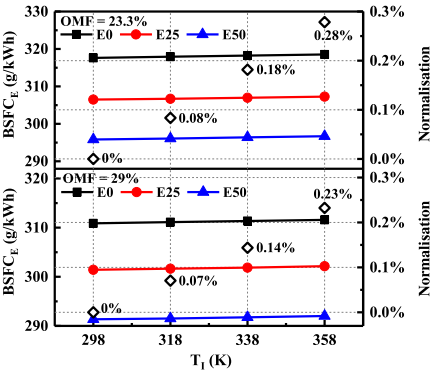

Figure 13. Effects of T_I on $BSFC_E$.

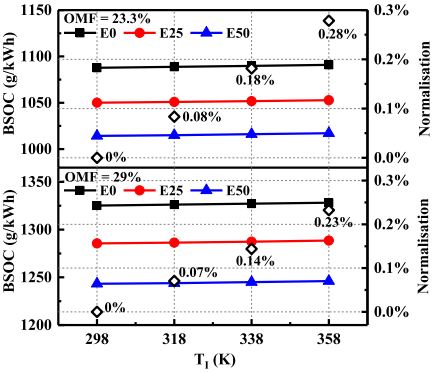

Figure 14. Effects of T_I on BSOC.

and OMF = 29%. This is mainly because the intake density will be reduced on increasing T_I under a fixed opening angle of engine throttle.

In the meantime, the combustion phasing will be slightly affected on changing T_I under E0, E25, and E50 fuel conditions. As shown in Figures 15 and 16, on increasing T_I from 298 to 358 K, θ_F and θ_C will be reduced by around 0.7°. φ_{CA50}, φ_{Pmax}, and the position of the HRR peak will be advanced by nearly 1°. This is principally because the atomization of fuel droplets could be enhanced with a higher temperature intake.

4. CONCLUSIONS

This work belongs to the "RIVER" project to develop a noncarbon riverboat powered by an ICE with conventional hydrocarbon liquid fuels, which is expected to make a valuable contribution to carbon neutrality in the world. The findings of

https://doi.org/10.1021/acsomega.1c02947
ACS Omega 2021, 6, 29394−29402

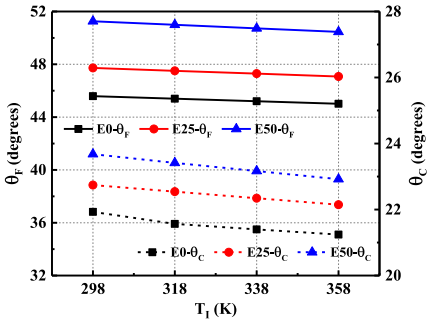

(a) OMF = 23.3%

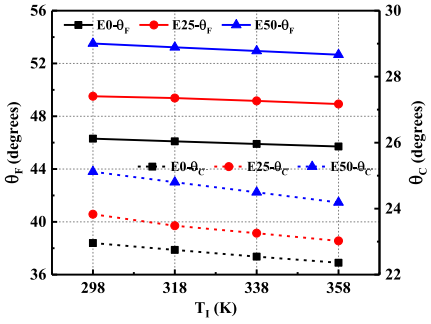

(b) OMF = 29%

Figure 15. Effects of T_I on θ_F, and θ_C.

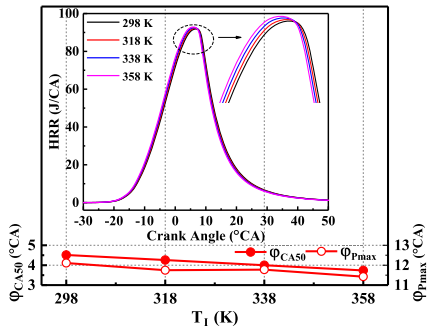

Figure 16. Effects of T_I on the HRR, φ_{CA50}, and φ_{Pmax} (E25; OMF = 23.3%).

this work not only provide a critical analysis on the implementation of OFC technology in a practical GDI engine fueled with gasoline−ethanol blends but also continue to contribute to this growing area by exploring the methods of improving the efficiency of OFC SI engines. The major conclusions in this article can be summarized as follows:

(1) $BSFC_E$, θ_F, and θ_C are sensitive to spark timing under OFC mode for all of the fuel conditions (E0, E25, and E50).

(2) With a fixed spark timing, the φ_{CA50} of E50 and E25 is about 4.5 and 1.9° later than that of E0, respectively. θ_F and θ_C can be extended by increasing the ethanol fraction in the blended fuel.

(3) With MBT timing under each OMF condition and by increasing the OMF from 23.3 to 29%, the saving rate of $BSFC_E$ is 2.12, 1.65, and 1.51% for E0, E25, and E50, respectively. The corresponding increase in BSOC is 21.83, 22.42, and 22.58%, respectively, which should also increase the attention in practical applications.

(4) θ_F, θ_C, and HRR are not sensitive to the OMF. With the increase of the OMF, the increment of θ_F is 0.7, 1.8, and 2.2° for E0, E25, and E50, respectively. θ_C is only extended by 1, 1.1, and 1.4°, respectively.

(5) By increasing T_I from 298 to 358 K, $BSFC_E$ and BSOC present steady but slight growth trends under all of the fuel conditions. θ_F and θ_C could be slightly reduced, while φ_{CA50}, φ_{Pmax}, and the position of HRR peak could be advanced by nearly 1°.

In the future, more research on OFC in GDI engines fueled with gasoline−ethanol blends would be beneficial. For example, further studies could include other new parameters, such as the effects of variable valve actuation strategies, exhaust gas recirculation (EGR), intake pressure and temperatures, fuel injection rate and pressure, etc. Besides, the studies about combustion performance under some other representative load points can also be considered. Thus, future works can further benefit the implementation of OFC in GDI engines fueled with gasohol, providing a practical and meaningful way to help achieve zero carbon emissions from ICE.

AUTHOR INFORMATION

Corresponding Authors

Xiang Li − *School of Computer Science and Technology, University of Bedfordshire, Luton LU1 3JU, U.K.*; orcid.org/0000-0002-4442-9330; Email: xiang.li@beds.ac.uk

Zhijun Peng − *School of Engineering, University of Lincoln, Lincoln LN6 7TS, U.K.*; Email: jpeng@lincoln.ac.uk

Authors

Yiqiang Pei − *State Key Laboratory of Engines, Tianjin University, Tianjin 300072, China*

Dayou Li − *School of Computer Science and Technology, University of Bedfordshire, Luton LU1 3JU, U.K.*

Tahmina Ajmal − *School of Computer Science and Technology, University of Bedfordshire, Luton LU1 3JU, U.K.*

Abdel Aitouche − *Univ. Lille, CNRS, Centrale Lille, UMR 9189 - CRIStAL - Centre de Recherche en Informatique Signal et Automatique de Lille, F-59000 Lille, France; Junia, Smart Systems and Energies, F-59000 Lille, France*

Raouf Mobasheri − *Univ. Lille, CNRS, Centrale Lille, UMR 9189 - CRIStAL - Centre de Recherche en Informatique Signal et Automatique de Lille, F-59000 Lille, France; Junia, Smart Systems and Energies, F-59000 Lille, France*

Complete contact information is available at: https://pubs.acs.org/10.1021/acsomega.1c02947

Notes

The authors declare no competing financial interest.

ACKNOWLEDGMENTS

This work was financially supported by the European Regional Development Fund (ERDF) via Interreg North-West Europe (Project No. NWE553).

ABBREVIATIONS

BMEP	brake mean effective pressure
BSFC	brake-specific fuel consumption
CA	crank angle
CAC	conventional air combustion
CCS	carbon capture and storage
CO_2	carbon dioxide
E0	gasoline

https://doi.org/10.1021/acsomega.1c02947
ACS Omega 2021, 6, 29394−29402

E25	25% ethanol, 75% is gasoline in mass fraction
E50	50% ethanol, 50% is gasoline in mass fraction
ECU	electronic control unit
EGR	exhaust gas recirculation
ERDF	European regional development fund
GDI	gasoline direct injection
GHG	greenhouse gas
HRR	heat release rate
ICE	internal combustion engine
ICRC	internal combustion Rankine cycle
KLSA	knock-limited spark advance
MBT	maximum brake torque
OFC	oxy-fuel combustion
OMF	oxygen mass fraction
PFI	port fuel injection
rpm	revolutions per minute
SI	spark ignition

REFERENCES

(1) Salvia, M.; Reckien, D.; Pietrapertosa, F.; Eckersley, P.; Spyridaki, N. A.; Krook-Riekkola, A.; Olazabal, M.; Hurtado, S. D. G.; Simoes, S. G.; Geneletti, D.; et al. Will climate mitigation ambitions lead to carbon neutrality? An analysis of the local-level plans of 327 cities in the EU. *Renewable Sustainable Energy Rev.* **2021**, *135*, No. 110253.

(2) Koytsoumpa, E. I.; Bergins, C.; Kakaras, E. The CO_2 economy: Review of CO_2 capture and reuse technologies. *J. Supercrit. Fluids* **2018**, *132*, 3−16.

(3) Anwar, M. N.; Fayyaz, A.; Sohail, N. F.; Khokhar, M. F.; Baqar, M.; Khan, W. D.; Rasool, K.; Rehan, M.; Nizami, A. S. CO2 capture and storage: a way forward for sustainable environment. *J. Environ. Manage.* **2018**, *226*, 131−144.

(4) Zheng, G.; Peng, Z. Life Cycle Assessment (LCA) of BEV's environmental benefits for meeting the challenge of ICExit (Internal Combustion Engine Exit). *Energy Rep.* **2021**, *7*, 1203−1216.

(5) Yaverbaum, L. *Fluidized Bed Combustion of Coal and Waste Materials*, NASA STI/Recon Technical Report A, 1977; Vol. 78, p 33803.

(6) Bilger, R. W. In *Zero Release Combustion Technologies and the Oxygen Economy*, Fifth International Conference on Technologies and Combustion for a Clean Environment, Lisbon, Portugal, July, 1999; pp 12−15.

(7) Wu, H. W.; Wang, R. H.; Chen, Y. C.; Ou, D. J.; Chen, T. Y. Influence of port-inducted ethanol or gasoline on combustion and emission of a closed cycle diesel engine. *Energy* **2014**, *64*, 259−267.

(8) Li, X.; Peng, Z.; Ajmal, T.; Aitouche, A.; Mobasheri, R.; Pei, Y.; Gao, B.; Wellers, M. A feasibility study of implementation of oxy-fuel combustion on a practical diesel engine at the economical oxygen-fuel ratios by computer simulation. *Adv. Mech. Eng.* **2020**, *12*, 1−13.

(9) Wall, T.; Liu, Y.; Spero, C.; Elliott, L.; Khare, S.; Rathnam, R.; Zeenathal, F.; Moghtaderi, B.; Buhre, B.; Sheng, C.; et al. An overview on oxyfuel coal combustion—State of the art research and technology development. *Chem. Eng. Res. Des.* **2009**, *87*, 1003−1016.

(10) Chen, L.; Yong, S. Z.; Ghoniem, A. F. Oxy-fuel combustion of pulverized coal: Characterization, fundamentals, stabilization and CFD modeling. *Prog. Energy Combust. Sci.* **2012**, *38*, 156−214.

(11) Yu, X.; Wu, Z.; Wang, C.; Deng, J.; Hu, Z.; Li, L. In *Study of the Combustion and Emission Characteristics of a Quasi ICRC Engine under Different Engine Loads*, SAE Technical Paper 2014-01-1202, SAE, 2014.

(12) Fu, L. Z.; Wu, Z.; Li, L.; Yu, X. In *Effect of Water Injection Temperature on Characteristics of Combustion and Emissions for Internal Combustion Rankine Cycle Engine*, SAE Technical Paper 2014-01-2600, SAE, 2014.

(13) Wu, Z. J.; Yu, X.; Fu, L. Z.; Deng, J.; Hu, Z. J.; Li, L. G. A high efficiency oxyfuel internal combustion engine cycle with water direct injection for waste heat recovery. *Energy* **2014**, *70*, 110−120.

(14) Wu, Z. J.; Yu, X.; Fu, L. Z.; Deng, J.; Li, L. G. Experimental study of the effect of water injection on the cycle performance of an internal-combustion Rankine cycle engine. *Proc. Inst. Mech. Eng., Part D* **2014**, *228*, 580−588.

(15) Li, X.; Peng, Z.; Ajmal, T.; Rana, K. J.; Aitouche, A.; Mobasheri, R.; Pei, Y. In *Simulation Study on Implementation of Oxy-Fuel Combustion for a Practical GDI Engine*, SAE Technical Paper 2021-01-0380, SAE, 2021.

(16) Li, X.; Pei, Y.; Peng, Z.; Ajmal, T.; Rana, K. J.; Aitouche, A.; Mobasheri, R. Numerical study on the effects of intake charge on oxy-fuel combustion in a dual-injection spark ignition engine at economical oxygen-fuel ratios *Int. J. Engine Res.* 2021, DOI: 10.1177/14680874211022292.

(17) An, Y.; Teng, S.; Li, X.; Qin, J.; Zhao, H.; Zhan, Z. S.; Hu, T. G.; Liu, B.; Zhong, J. In *Study of Polycyclic Aromatic Hydrocarbons Evolution Processing in GDI Engines using TRF-PAH Chemical Kinetic Mechanism*, SAE Technical Paper 2016-01-0690, SAE, 2016.

(18) Wu, M.; Pei, Y.; Qin, J.; Li, X.; Zhou, J.; Zhan, Z. S.; Guo, Q. Y.; Liu, B.; Hu, T. G. In *Study on Methods of Coupling Numerical Simulation of Conjugate Heat Transfer and In-cylinder Combustion Process in GDI Engine*, SAE Technical Paper 2017-01-0576, SAE, 2017.

(19) Kim, T.; Song, J.; Park, J.; Park, S. Numerical and experimental study on effects of fuel injection timings on combustion and emission characteristics of a direct-injection spark-ignition gasoline engine with a 50 MPa fuel injection system. *Appl. Therm. Eng.* **2018**, *144*, 890−900.

(20) Duronio, F.; De Vita, A.; Allocca, L.; Anatone, M. Gasoline direct injection engines−A review of latest technologies and trends. Part 1: Spray breakup process. *Fuel* **2020**, *265*, No. 116948.

(21) Wang, C.; Pei, Y.; Qin, J.; Peng, Z.; Liu, Y.; Xu, K.; Ye, Z. Laser induced fluorescence investigation on deposited fuel film from spray impingement on viscous film over a solid wall. *Energy* **2021**, *231*, No. 120893.

(22) Choi, Y.; Yi, H.; Oh, Y.; Park, S. Effects of engine restart strategy on particle number emissions from a hybrid electric vehicle equipped with a gasoline direct injection engine. *Atmos. Environ.* **2021**, *253*, No. 118359.

(23) Wang, Z.; Liu, H.; Long, Y.; Wang, J.; He, X. Comparative study on alcohols−gasoline and gasoline−alcohols dual-fuel spark ignition (DFSI) combustion for high load extension and high fuel efficiency. *Energy* **2015**, *82*, 395−405.

(24) Huang, H.; Wang, Q.; Shi, C.; Liu, Q.; Zhou, C. Comparative study of effects of pilot injection and fuel properties on low temperature combustion in diesel engine under a medium EGR rate. *Appl. Energy* **2016**, *179*, 1194−1208.

(25) Huang, H.; Teng, W.; Li, Z.; Liu, Q.; Wang, Q.; Pan, M. Improvement of emission characteristics and maximum pressure rise rate of diesel engines fueled with n-butanol/PODE3-4/diesel blends at high injection pressure. *Energy Convers. Manage.* **2017**, *152*, 45−56.

(26) Li, X.; Pei, Y. Q.; Qin, J.; Zhang, D.; Wang, K.; Xu, B. Effect of ultra-high injection pressure up to 50 MPa on macroscopic spray characteristics of a multi-hole gasoline direct injection injector fueled with ethanol. *Proc. Inst. Mech. Eng., Part D* **2018**, *232*, 1092−1104.

(27) Huang, H.; Liu, Q.; Teng, W.; Pan, M.; Liu, C.; Wang, Q. Improvement of combustion performance and emissions in diesel engines by fueling n-butanol/diesel/PODE3−4 mixtures. *Appl. Energy* **2018**, *227*, 38−48.

(28) Venu, H.; Raju, V. D.; Subramani, L. Combined effect of influence of nano additives, combustion chamber geometry and injection timing in a DI diesel engine fuelled with ternary (diesel-biodiesel-ethanol) blends. *Energy* **2019**, *174*, 386−406.

(29) Huang, H.; Zhu, Z.; Chen, Y.; Chen, Y.; Lv, D.; Zhu, J.; Ouyang, T. Experimental and numerical study of multiple injection effects on combustion and emission characteristics of natural gas−diesel dual-fuel engine. *Energy Convers. Manage.* **2019**, *183*, 84−96.

(30) Holman, J. P. *Experimental Methods for Engineers*; Mc Grawhill, 1966.

https://doi.org/10.1021/acsomega.1c02947
ACS Omega 2021, 6, 29394−29402

(31) Liu, K.; Li, Y.; Yang, J.; Deng, B.; Feng, R.; Huang, Y. Comprehensive study of key operating parameters on combustion characteristics of butanol-gasoline blends in a high speed SI engine. *Appl. Energy* **2018**, *212*, 13−32.
(32) Tornatore, C.; Bozza, F.; De Bellis, V.; Teodosio, L.; Valentino, G.; Marchitto, L. Experimental and numerical study on the influence of cooled EGR on knock tendency, performance and emissions of a downsized spark-ignition engine. *Energy* **2019**, *172*, 968−976.
(33) Tian, Z.; Zhen, X.; Wang, Y.; Liu, D.; Li, X. Combustion and emission characteristics of n-butanol-gasoline blends in SI direct injection gasoline engine. *Renewable Energy* **2020**, *146*, 267−279.
(34) Woschni, G. In *A Universally Applicable Equation for the Instantaneous Heat Transfer Coefficient in the Internal Combustion Engine*, SAE Technical Paper 670931, SAE, 1967.
(35) Heywood, J. B. *Internal Combustion Engine Fundamentals*, 2nd ed.; McGraw-Hill, 2018.
(36) Metghalchi, M.; Keck, J. C. Burning velocities of mixtures of air with methanol, isooctane, and indolene at high pressure and temperature. *Combust. Flame* **1982**, *48*, 191−210.

https://doi.org/10.1021/acsomega.1c02947
ACS Omega 2021, 6, 29394−29402